ENCLOSURE 4

M210152

Licensing Topical Report

NEDO-33922, Revision 2, BWRX-300 Containment Evaluation Method

Non-Proprietary Information

IMPORTANT NOTICE

This is a non-proprietary version of the BWRX-300 Containment Evaluation Method Licensing Topical Report, from which the proprietary information has been removed. The header of each page in this enclosure carries the notation "Non-Proprietary Information." Portions of the enclosure that have been removed are indicated by an open and closed bracket as shown here [[ ]].

HITACHI

GE Hitachi Nuclear Energy

NEDO-33922
Revision 2
December 2021

Non-Proprietary Information

Licensing Topical Report

BWRX-300 Containment Evaluation Method

Copyright 2021 GE-Hitachi Nuclear Energy Americas, LLC

All Rights Reserved

INFORMATION NOTICE

This is a non-proprietary version of the GE Hitachi Nuclear Energy (GEH) document NEDC-33922P Revision 2, which has the proprietary information removed. Portions of the document that have been removed are indicated by an open and closed bracket as shown here [[ ]].

IMPORTANT NOTICE REGARDING CONTENTS OF THIS REPORT

Please Read Carefully

The design, engineering, and other information contained in this document is furnished for the purpose of obtaining Nuclear Regulatory Commission (NRC) review and determination of acceptability for use for the BWRX-300 design and licensing basis information contained herein. The only undertakings of GEH with respect to information in this document are contained in the contracts between GEH and its customers or participating utilities, and nothing contained in this document shall be construed as changing those contracts. The use of this information by anyone for any purpose other than that for which it is intended is not authorized; and with respect to any unauthorized use, GEH makes no representation or warranty, and assumes no liability as to the completeness, accuracy, or usefulness of the information contained in this document.

TABLE OF CONTENTS

LIST OF TABLES

LIST OF FIGURES

REVISION SUMMARY

Revision Number	Description of Change
0	Initial Submittal
1	Revised to incorporate the following responses to NRC Requests for Additional Information (eRAIs): • NRC eRAI 9829 Question 06.02.04-01 revised Section 1.3. • NRC eRAI 9831 Question 06.02.01-02 revised Section 6.11. • NRC eRAI 9862 Question 06.02.01-01 added a new Section 1.4 and Table 6-6 and revised Sections 6.0, 6.10.1 and 6.10.2. • NRC eRAI 9862 Question 06.02.01-02 revised Section 6.10.2 and added Figures 6-39 to 6-41. • NRC eRAI 9862 Question 06.02.01-03 revised Sections 6.5, 6.6.1, 6.6.2, 6.10, 6.10.2 and 6.11 and revised Figures 6-26, 6-28, and 6-31. • NRC eRAI 9862 Question 06.02.01-05 revised Sections 6.10.2 and 6.11. • NRC eRAI 9862 Question 06.02.01-07 revised several figures. • NRC eRAI 9862 Question 06.02.01-08 revised Sections 6.5 and 6.8.2. Revised in response to the following Audit Issues: • Audit Issue 2 revised Figures 6-31 through 6-34. • Audit Issue 26 corrected Figures 5-3 and 5-4. • Audit Issue 30 revised Section 6.9 and clarified the legends in Figures 6-23, 6-24, and 6-25. • Audit Issue 35 corrected a broken link in Section 6.9. • Audit Issue 36 deleted all references to a design option in Sections 2.0 and 6.1 and Table 6-2. • Audit Issue 45 revised Section 6.5 and 6.8.2 to describe the steam dome biases in more detail. In general, the following figures were updated to reflect updated results: Figure 5-1, Figures 5-3 through 5-27, Figures 6-1, 6-4 through 6-10, 6-13, 6-16, 6-23 through 6-34, and 6-38 through 6-41. A new figure, Figure 6-42, was added. Because of the revisions noted above, the following additional revisions occurred:

Revision Number	Description of Change
	• Figures 6-39 and 6-40 were renumbered as Figures 6-43 and 6-44. • Section 6.10.3: Figure references were updated to reflect that Figures 6-39 and 6-40 were renumbered as Figures 6-43 and 6-44. The following additional editorial corrections were made: • Section 5.2.4: Added back in the missing equation for the radiolytic gas production correlation. • Corrected broken links in Sections 4.0, 6.0, 6.8, 6.8.2, 6.9, 6.10, and 6.11.
2	Revised the following tables, figures, and sections consistent with the revised response to NRC eRAI 9862 Question 06.02.01-01: • Table 6-6 • Figure 6-2 • Figures 6-4 through 6-13 • Figures 6-15 through 6-17 • Figures 6-26 through 6-44 • Sections 6.5, 6.6.1, 6.6.2, 6.7.1, 6.7.2, 6.10.1, 6.10.2, and 6.11. Section 5.2.4: Added a sentence to the first paragraph in response to Audit Issue 38. Section 6.8.2: Deleted the reference to CONAN test data. The following additional editorial corrections were made: • Figures 5-3 and 5-4: Corrected the clarity of the images. • Figures 5-5, 5-8, 5-11, 5-15, 5-18, and 5-23: In the notes below these figures, added quotations around Q IC-A and Q IC-B for clarity. • Figure 5-11: Revised the note to delete Q IC-B. • Figures 5-8, 5-15, 5-18, and 5-23: Removed proprietary markings in the notes below the figures. • Sections 5.2.4, 5.2.5, 5.3.1, 6.7.2, 6.8, 6.8.1, 6.8.3, and 6.10.1 and in Table 5-3 and Table 6-2 (Items 8, 9, 12, 13, and 14): Added the missing article “the” in several places. • Table 6-2 (Items 14 and 21): Changed “effects” to “affects”. • Section 6.10.1: Deleted the word “one”. It is redundant with the word “first” • Section 6.10.3: Changed “is” to “are”.

Acronyms and Abbreviations

Term	Definition
ABWR	Advanced Boiling Water Reactor
AC	Alternating Current
ALARA	As Low As Reasonably Achievable
AOO	Anticipated Operational Occurrence
ASME	American Society of Mechanical Engineers
ATWS	Anticipated Transient Without Scram
B&PV	Boiler & Pressure Vessel
BDBA	Beyond Design Basis Accident
BTP	Branch Technical Position
BWR	Boiling Water Reactor
COL	Combined Operating License
CP	Construction Permit
CSAU	Code, Scaling, Applicability and Uncertainty
DCA	Design Certification Application
ECCS	Emergency Core Cooling System
EFCV	Excess Flow Check Valve
EMDAP	Evaluation Model Development and Assessment Process
ESBWR	Economic Simplified Boiling Water Reactor
GDC	General Design Criteria
GEH	GE Hitachi Nuclear Energy
GOTHIC	Generation of Thermal-Hydraulic Information for Containments
HGNE	Hitachi-GE Nuclear Energy Ltd.
HT	Heat Transfer
I&C	Instrumentation and Control
IC	Isolation Condenser
ICS	Isolation Condenser System
IE	Infrequent Event
LOCA	Loss-of-Coolant Accident
LOOP	Loss of Offsite Power

Term	Definition
LTR	Licensing Topical Report
LWR	Light Water Reactor
NBS	Nuclear Boiler System
NC	Non-Condensable
NRC	Nuclear Regulatory Commission
OL	Operating License
PCCS	Passive Containment Cooling System
PIRT	Phenomena Identification and Ranking Table
PSAR	Preliminary Safety Analysis Report
RCPB	Reactor Coolant Pressure Boundary
RCS	Reactor Coolant System
RG	Regulatory Guide
RPS	Reactor Protection System
RPV	Reactor Pressure Vessel
RWCU	Reactor Water Clean Up
SDC	Shut Down Cooling
SMR	Small Modular Reactor
SRP	Standard Review Plan
SSC	Structure, System, and Component
TAF	Top of Active Fuel
TMI	Three Mile Island
TRACG	Transient Reactor Analysis Code General Electric

1.0 INTRODUCTION

1.1 Purpose

This report presents the analysis method used for the BWRX-300 containment thermal hydraulics performance to demonstrate that the containment design satisfies the acceptance criteria listed in Section 4.0 of Licensing Topical Report (LTR) NEDC-33911P, BWRX-300 Containment Performance (Reference 7.2).

The containment analysis method is outlined in Section 3.0 of NEDC-33911P (Reference 7.2). The scope of the evaluation method are the design basis and special events that are evaluated to establish the suitability of the containment performance acceptance criteria:

- Anticipated Operational Occurrences (AOOs)
- Station Blackout as required by 10 CFR 50.63
- Anticipated Transients Without Scram (ATWS) as required by 10 CFR 50.62
- Large Break Loss of Coolant Accident (LOCA) inside containment
- Small Break LOCA inside containment

1.2 Scope of Application

This report scope includes:

- Method description
- Method qualification
- Sensitivity studies
- Application of the method to the BWRX-300 for the events identified in Section 1.1
- Demonstration cases

Because the BWRX-300 Reactor Pressure Vessel and Isolation Condensers System (ICS) are similar to those of the Economic Simplified Boiling Water Reactor (ESBWR), the TRACG method developed for the ESBWR reactor pressure vessel (RPV) thermal hydraulics and mass and energy release is also used for the BWRX-300 RPV thermal hydraulics and mass and energy release. This report provides an overview of the TRACG thermal hydraulics method for the mass and energy release and its applicability to the BWRX-300 RPV.

The containment analysis is performed by using the GOTHIC code (Reference 7.16). The development outline for the GOTHIC containment evaluation method is given in Section 3.4.2 of NEDC-33911P utilizing the applicable elements of the Code, Scaling, Applicability, and Uncertainty (CSAU) framework.

The application of TRACG and GOTHIC for the BWRX-300 containment includes a base case using nominal inputs and assumptions, and a conservative case using inputs and assumptions that are biased to bound the uncertainties.

[[

]] The

subcompartments are included in the analyses to determine the containment atmosphere remains sufficiently well mixed to preclude deflagration or detonation of combustible gases, and to demonstrate that the containment internal structures forming the boundaries of the subcompartments do not experience large pressure differentials [[ ]]. Jet loads that may be exerted on structures and equipment in containment are addressed as part of the structural loads evaluation that will be submitted in a future licensing submittal.

1.3 Acceptance Criteria

The evaluation method demonstrates that the BWRX-300 containment meets the following acceptance criteria:

- Accident pressure and temperature are less than design pressure and temperature with appropriate margin
- Containment pressure is reduced to less than 50% of the peak accident pressure for the most limiting LOCA within 24 hours
- Containment pressure responses after 24 hours for LOCAs that do not produce the peak accident pressure are maintained below 50% of the peak pressure for the most limiting LOCA
- Containment atmosphere remains sufficiently mixed such that deflagration or detonation does not occur inside containment

Containment venting or leakage shall not be credited for at least 72 hours in demonstrating that the above acceptance criteria are met during a design basis event or accident.

Regulatory Guides (RG) 1.203 (Reference 7.3) and RG 1.157 (Reference 7.4) provide guidance for acceptable evaluation methods applicable to light water reactors. RG 1.157 provides analyses guidance for demonstrating compliance to the fuel clad integrity requirements of 10 CFR 50.46 “Acceptance criteria for emergency core cooling systems in light water nuclear power reactors”. The BWRX-300 LOCA sequences do not progress into significant core uncovery and refill/reflooding. BWRX-300 LOCAs do not result in significant fuel heat-up and oxidation and are not mitigated by an active injection system. Therefore, most RG 1.157 guidance are not applicable to the BWRX-300 LOCA analyses. Only the RG 1.157 guidance relating to the general best practice elements of a rigorous method development are applicable. These best practice elements are also included in RG 1.203. RG 1.203 provides guidance for all elements and stages of developing an acceptable method and references the CSAU analysis methodology (Reference 7.12). The BWRX-300 containment analysis utilizes mature computer codes that have been widely reviewed and used. The application method presented in this LTR addresses conformance with the RG 1.203 elements that are applicable to those mature codes and the CSAU methodology.

1.4 Methodology Overview

TRACG calculates the mass and energy release from modeled breaks of various sizes and locations (Section 5.2.2). In all cases, atmospheric pressure is used for the TRACG pressure boundary condition at the break. This approach provides no credit for the back pressure from containment; consequently, the retained RPV inventory calculated by TRACG represents the minimum

condition as though the break occurred outside containment. Breaks inside containment would realistically experience back pressure from the containment which would reduce the mass and energy release calculated by TRACG once the break flow became unchoked; however, this effect is not treated explicitly because it would require two-way coupling between the TRACG calculation and the GOTHIC containment calculation. Instead, the methodology has only a one-way coupling with the mass and energy release rates conservatively calculated by TRACG supplied as inputs to the GOTHIC calculation up until the point in time when the containment and RPV pressures first match. Choked flow naturally satisfies the assumed one-way coupling because the calculated choked flow rate does not depend on the downstream pressure. Select TRACG inputs are specified (Section 5.2.5 and 5.2.6) so that mass and energy release rates will be conservatively calculated.

For large breaks, the rapid mass and energy release into the containment before the break is isolated leads to the highest containment peak pressure, which occurs at approximately the same time that the break is isolated. For large breaks, the containment shell is the dominant short term energy sink; heat transfer to the containment shell will cause the containment pressure to decrease from its peak value after isolation of the break occurs. The large steam line break determines the overall highest peak containment pressure as shown by the demonstration calculations provided in Section 6.10.

Compared to the large breaks, small unisolated breaks have a much slower mass and energy release rate from the RPV into the containment. The lowest break on the RPV that remains unisolated and occurs outside the containment will produce the most limiting scenario for minimum RPV inventory. Regardless of break location and whether the break is inside or outside containment, the break flow will slowly decrease with time because the RPV is being depressurized largely by the ICS operation with some contribution from the energy released in the break flow. The containment pressure will slowly increase and eventually equal the RPV pressure if the break is inside containment. After the point in time when the containment and RPV pressures first become equal, it is no longer realistic to use the TRACG break flow that was calculated using an atmospheric pressure boundary condition as input to the GOTHIC containment calculation. The methodology does not require the GOTHIC calculation to continue beyond the point where the containment and RPV pressures equalize because the longer-term containment pressure will be bounded by the RPV pressure calculated by assuming zero break flow provided that the PCCS is depressurizing containment faster than the ICS is depressurizing the RPV for the case of zero break flow beyond the intersection time.

2.0 OVERVIEW OF THE BWRX-300 RPV AND CONTAINMENT FEATURES PERTINENT TO THE APPLICATION METHOD

The BWRX-300 RPV and internals are shown on Figure 2-1 and described in Reference 7.1. The Isolation Condensers (IC) are also described in Reference 7.1 with illustrations included on Figure 2-2 and Figure 2-3. As described in Reference 7.1, all piping [[

]]. For an ICS train, the RPV isolation valves on both the steam and condensate pipes for that train close when a break is detected in that train. All other RPV isolation valves close on detection of high drywell pressure. Isolation condensers are initiated on [[

]]. The other isolation and initiations signals are described in References 7.1 and 7.2 and not repeated here because they are not pertinent to the containment thermal-hydraulic response analyses.

A conceptual containment design, penetrations and Passive Containment Cooling System (PCCS) are also described in Reference 7.2. As stated in NEDC-33911P, the containment structure, shape and PCCS design may be different, but the containment design would be functionally the same. The containment conceptual design has evolved subsequent to the issuance of Reference 7.2. The containment shape shown on Figure 2-4 is the configuration used in the method development because [[

]]. Regardless of the type of the vessel support, it is necessary that the support structure has large openings for personnel access and maintenance or replacement of the control blades and control rod drives.

Containment penetrations and containment isolation valves are also discussed in Reference 7.2.

The following containment design features are relevant to the purposes of this report:

- Containment is a dry enclosure, near atmospheric pressure during normal operation
- Containment design pressure and temperature are within the experience base of conventional BWRs
- Containment is inerted with nitrogen during normal operation
- There are no subcompartments containing large bore high energy lines
- The subcompartments have sufficiently large openings such that the boundaries of the subcompartments do not experience large pressure differentials resulting from pipe breaks outside the subcompartments.
- The PCCS [[

]].

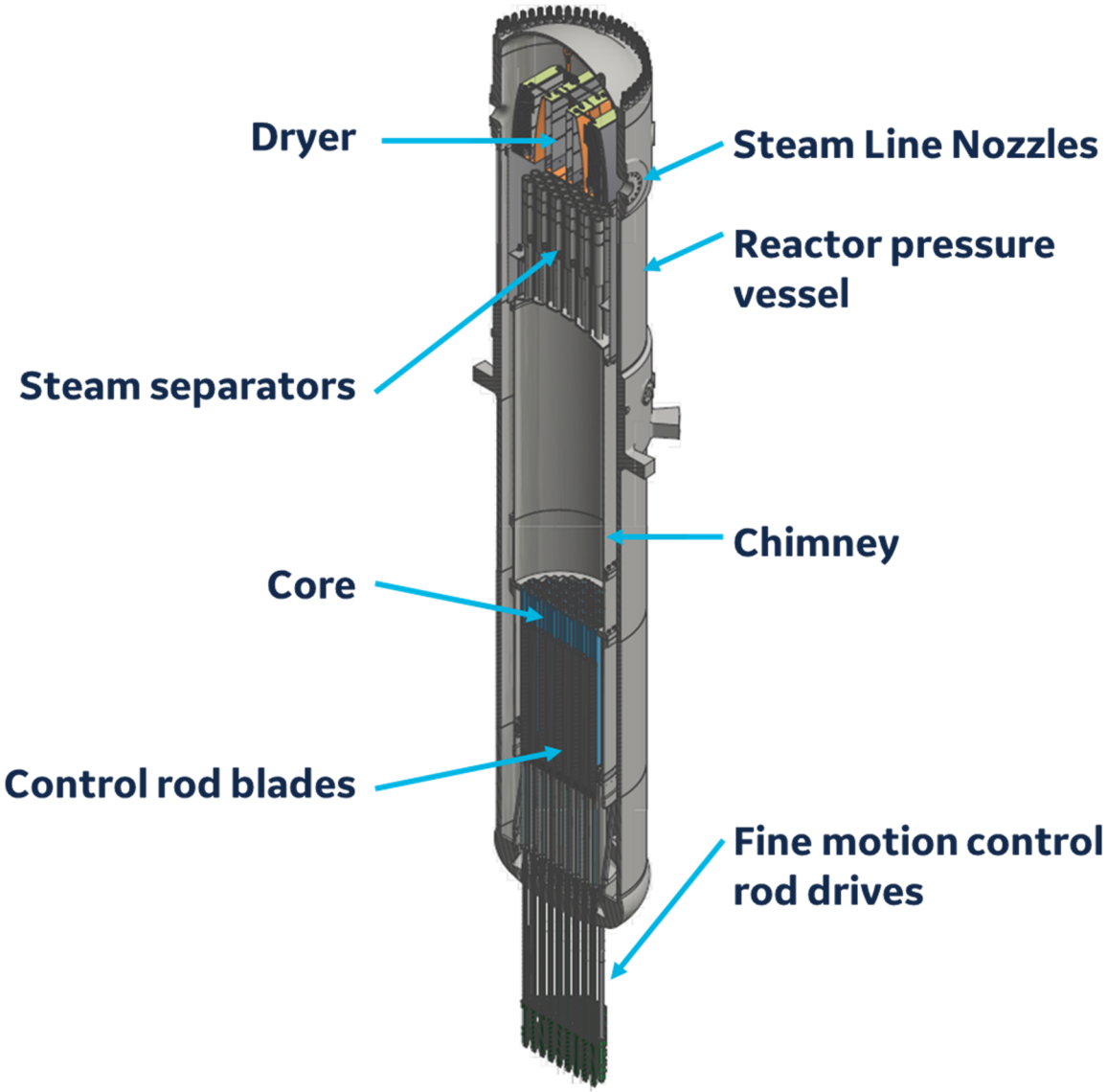

Figure 2-1: BWRX-300 RPV and Internals

[[

]]

Figure 2-2: BWRX-300 Isolation Condenser System

[[

]]

Figure 2-3: Isolation Condenser CIVs Connected to the RPV Boundary

[[

]].

[[

]]

Figure 2-4: BWRX-300 Containment with PCCS Utilizing Concentric Pipes (typical configuration)

3.0 LOCA Scenarios and Limiting Pipe Breaks

All large bore piping attached to the BWRX-300 RPV has two isolation valves. The RPV isolation valves, except for those on the IC piping, close on either of the following conditions:

- High drywell pressure
- Low-Low RPV water level

The containment isolation valves also close on the same signals but may have a longer delay than the RPV isolation valves. The outboard containment isolation valves are assumed to remain open for a main steam pipe break, but the turbine stop valve is closed instantaneously, concurrent with the break. Because the two steam pipes are connected to a common header upstream of the turbine stop and control, the intact loop also contributes to the break flow rate before the RPV isolation valves are closed. Using this set of assumptions maximizes the discharge of steam to containment.

The feedwater pipes have a check valve outside containment. As a result, the intact feedwater loop does not feed backwards to the break. The feedwater pump trips on a pipe break. The hot water in the feedwater piping may flash and contribute to break flow.

Both the steam supply and the condensate return pipes of an IC train are also isolated when a break is detected on either pipe in that train. The IC condensate return pipe flow area is much smaller than the feedwater pipe; therefore, a break in the condensate piping in an IC train is bounded by the feedwater pipe breaks. The IC steam supply pipe flow area is no larger than the main steam pipe flow limiter flow area. Main steam pipe flow area is at least twice as large as the flow limiter flow area. Further, pipe inventory in the main steam piping is much larger than the inventory in an IC train and its attached piping. Therefore, the initial steam discharge rate following a main steam pipe break is significantly larger than the initial discharge rate from an IC steam pipe break.

The isolation signals for ICS pipe breaks are [[ ]] and do not require a high containment pressure signal. There is no inherent reason that isolation of ICS pipe breaks would be delayed further than isolation of other pipe breaks. Although there may be differences in electronic signal delays to develop for various pipe breaks, the isolation times considered in the analysis are bounding for all large pipe breaks. Considering the pipe size, configuration and isolation signal timing assumed in the analysis, a break in the ICS piping is bounded by a break in the main steam and / or feedwater pipe as analyzed.

Reactor water cleanup (RWCU) and shutdown cooling (SDC) pipes also have RPV isolation valves. Because the RWCU and shutdown cooling pipes are smaller in diameter than the feedwater pipes, and the isolation valve closure timing is the same for all pipes, breaks in the RWCU and SDC pipes are bounded by feedwater pipe breaks.

The inside diameters of the instrument lines are [[ ]]. These pipes are not isolated and assumed to discharge steam or liquid indefinitely. Also, the leak detection system in the ICS has a lower limit on the break size that it can detect. Such a break will remain unisolated even if the containment pressure exceeds the setpoint for isolation.

All small steam pipe breaks that remain unisolated are bounded by a break in a pipe of [[ ]] attached to the RPV dome.

All small liquid pipe breaks that remain unisolated are bounded by a break in a pipe of [[

]].

An assumed single failure rendering an ICS train inoperative is the most limiting single failure for small breaks because the small breaks rely on ICS to depressurize the RPV. [[

]].

In summary, the limiting large breaks are:

- Main steam pipe
- Feedwater pipe

All design basis large breaks are rapidly isolated at the RPV nozzle.

The limiting small breaks are unisolated instrument line breaks, either in the steam or liquid space.

4.0 OVERVIEW OF THE EVALUATION MODEL

TRACG is used to evaluate the mass and energy release from the BWRX-300 RPV, and GOTHIC is used to evaluate the BWRX-300 containment response. As shown in this report, there is no adverse effect of containment backpressure on the TRACG mass and energy releases. As a result, there is no need to iterate between the two codes to obtain a best estimate solution for the mass and energy release, and the application method is not dependent on predicting back pressure. Instead, mass and energy releases calculated by TRACG are used as a boundary condition in the GOTHIC calculations, and the containment pressure and temperature response are calculated using GOTHIC.

The mass and energy release model for the BWRX-300 containment response utilizes the applicable parts of the approved LTR, TRACG Application for ESBWR (Reference 7.10), which is incorporated in the approved ESBWR Design Certification (Reference 7.11). Section 5.0 of this report details the application of the ESBWR TRACG method to the BWRX-300.

As described in NEDC-33911P, Section 2.0, the BWRX-300 containment design is much simpler than the ESBWR containment, and many of the ESBWR containment phenomena do not apply to the BWRX-300 containment. Phenomena that are of secondary importance to the ESBWR containment response may become important to the BWRX-300 containment response. Therefore, a new containment model using GOTHIC has been developed for the BWRX-300 and is presented in this LTR. GOTHIC is a continuously maintained and improved computer code. The GOTHIC code has been developed compliant with 10 CFR 50, Appendix B requirements and meets the GEH software quality requirements. The results in this report have been generated using GOTHIC Version 8.3 that is the latest released version at this time. Future BWRX-300 containment analyses may be performed using newer versions of the GOTHIC code provided the newer versions meet the same 10 CFR50 Appendix B quality requirements and changes in calculated results for our BWRX-300 containment application caused by any code changes can be successfully dispositioned.

The evaluation method for the BWRX-300 containment response to design basis events has been developed following the applicable elements of Regulatory Guide 1.203 (Reference 7.3). The application method includes base cases and conservative cases. The individual key inputs, assumptions and modeling parameters are conservatively biased simultaneously in the conservative cases, rather than sampling the uncertainties and adding margin to the base case results. While this method compounds conservatisms, it gives reasonable assurance that the overall method results bound the uncertainties, and greatly reduces the number of sensitivity calculations. This is the same approach that was taken for the ESBWR containment method in Reference 7.10. The containment response method is described in detail in Section 6.

5.0 TRACG METHOD FOR MASS AND ENERGY RELEASE

5.1 TRACG Code and Qualification

TRACG is the GE Hitachi Nuclear (GEH) proprietary version of the Transient Reactor Analysis Code (TRAC). TRACG uses realistic one-dimensional and three-dimensional (3D) models and numerical methods to simulate phenomena that are experienced in the operation of boiling water reactors (BWRs). TRACG code and models are described in detail in Reference 7.5. The TRACG qualification report, Reference 7.6, includes comparisons of TRACG calculations with data from separate effects, component performance and integral system effects tests that directly support its use for BWR LOCA analyses. References 7.7 and 7.8 present TRACG qualification specifically for natural circulation plants with IC systems similar to the BWRX-300.

TRACG ECCS-LOCA analysis method for BWR/2–6 (Reference 7.9) and for ESBWR (Reference 7.10) have been approved previously. The uncertainties in the TRACG ECCS-LOCA analysis methods are quantified for the BWR/2-6 application method in Reference 7.9, and for ESBWR in Reference 7.10. It should be noted that only the uncertainties relating to RPV inventory and break flow would be accounted for in the BWRX-300 application because like the ESBWR application, the core always remains well cooled.

5.2 Application of the ESBWR TRACG LOCA Method to BWRX-300 Mass and Energy Release Calculations

The BWRX-300 RPV is an evolution of the ESBWR RPV. The main differences between the BWRX-300 RPV and ESBWR RPV are the RPV dimensions, connected piping, and the RPV isolation functions. These differences affect the modeling inputs but are still within the same qualified application range as the ESBWR. The BWRX-300 operating accident pressure and temperature ranges are similar to the ESBWR operating pressure and temperature ranges.

As discussed in this LTR, significant fuel heat-up does not occur in the BWRX-300 as is the case for the ESBWR. The phenomena that affect the mass and energy release from the BWRX-300 RPV case also apply to the ESBWR mass and energy release. The modeling, experimental and scaling uncertainties identified for ESBWR are also relevant to the BWRX-300 design. Therefore, the TRACG qualification for the ESBWR application equally applies to the BWRX-300 application. Furthermore, the BWRX-300 mass and energy release analysis is much less challenging than the ESBWR analysis for mass and energy release from a large break because the BWRX-300 large breaks are isolated. Small breaks are slow evolving events where the modeling and phenomenological uncertainties are significantly diminished.

In the BWRX-300, the RPV is isolated following a large break LOCA. After the isolation valves closure, the energy generated by decay heat must be removed directly from the RPV. Therefore, it is not appropriate to make the same assumptions as were made for the ESBWR where the PCCS is credited as the primary heat removal for ECCS-LOCA and containment analyses, while the ICS is credited for transients, but not for ECCS-LOCA or containment analyses. The BWRX-300 ICS is credited in accordance with its purpose, specification, and safety classification. The BWRX-300 ICs modeling and TRACG qualification are discussed in detail in Section 5.2.4.

The ESBWR TRACG LOCA method in Reference 7.10 includes ECCS-LOCA analysis and containment analysis. The TRACG models used for these analyses have some differences. The TRACG RPV model used for the ECCS-LOCA analysis (Figure 2.7-1 of Reference 7.10) is more

detailed with respect to the nodalization than the TRACG RPV model used for the ESBWR LOCA/Containment analysis (Section 3.7-1 of Reference 7.10). The axial detail in the RPV model is essentially equivalent for the BWRX 300 and ESBWR.

5.2.1 TRACG RPV Nodalization for BWRX-300

The TRACG RPV radial nodalization for the ESBWR ECCS LOCA analysis, shown on Figure 2.7-1 of Reference 7.10, is more detailed than the TRACG RPV radial nodalization used for the ESBWR analysis, shown on Figure 3.7-1 of Reference 7.10. Although either nodalization would be adequate for the BWRX 300 mass and energy release calculations, the demonstration cases presented in this LTR use a finer nodalization as shown on Figure 5-2. This refinement allows the use of the same RPV model both in transient and LOCA analyses.

Although the IC model developed for ESBWR is adequate for the BWRX-300 LOCA analyses, the IC model used in the BWRX-300 demonstration cases (Figure 5-4) is more detailed than the one used in the ESBWR analyses. This refinement was made for transient and ATWS analyses that are not in the scope of this report. The model on Figure 5-4 also reproduces the ESBWR IC specification heat removal rate for a single IC train. Only train A is shown on Figure 5-4, the other trains are modeled similarly.

5.2.2 Large and Small Pipe Breaks

The steam and feedwater piping attached to the RPV are shown on Figure 5-3. The large breaks are represented by [[

]].

5.2.3 Channel Grouping, Decay Heat and Power Shape

Containment analyses are not sensitive to the power shape and [[ ]]. These inputs are more relevant to the fuel heat-up calculations and transient analyses. [[

]].

5.2.4 Isolation Condenser Modeling and Radiolytic Gases

The IC capacity is assured to be at least 33.75 MW as stated in Supplement 2 of Reference 7.10. Although the ICS is credited for the AOOs in the ESBWR (Section 4.7 and Supplement 2 of Reference 7.10), but not for LOCA analyses, any potential adverse effects and parallel unit effects have been addressed in Reference 7.10. [[

]] The ESBWR containment analyses credit the PCCS attached to the containment, but do not credit the ICS. However, the ESBWR PCCS heat

exchanger is identical to one of the two heat exchangers in an IC train. Both the ICS and the PCCS use the same qualification base and testing that were originally performed for the Simplified Boiling Water Reactor (SBWR) design and supplemented for ESBWR design.

TRACG qualification for the ICS is based on two sets of PANDA tests as described in Reference 7.7: the M-series tests, which are used in the TRACG qualification for SBWR, and the later complimentary P-series tests for ESBWR configuration, including the effects of the non-condensable gases. TRACG04 is qualified based on both sets of tests, and for both water and steam, and steam containing air or helium (Reference 7.8).

Because there is no significant oxidation in the BWRX-300, the only non-condensable gases that may migrate into the IC tubes are the radiolysis products following a design basis LOCA. [[

]] The build-up of hydrogen and oxygen in steam following a one-inch liquid break is shown on Figure 5-1.

Unlike hydrogen generated from cladding oxidation, hydrogen and oxygen liberate from radiolysis at a slow rate and distributes over a relatively large region. The gases become mixed in water both in steam and liquid phases. The well-mixed hydrogen and oxygen in steam also migrates into the ICs when the ICs are put in service. The hydrogen and oxygen concentration in steam may increase as the steam condenses in the IC tubes. It should be noted that because hydrogen and oxygen are mixed in water when they are formed near the core region, they do not separate from water or steam again until the steam condenses.

The effect of the radiolytic gases on the ICs has been determined using TRACG. [[

]] Nevertheless, a bias was applied to the IC performance to account for degradation due to the potential of radiolytic gas build-up.

[[

]]

Figure 5-1: Volume Fraction of Radiolytic Gases ($H_2 + O_2$) in Steam in the RPV Following a 1-Inch Liquid Break

5.2.5 Modeling Biases (PIRTs)

TRACG has a feature to bias various modeling parameters, which are called PIRTs. A TRACG PIRT is a coefficient which multiplies an internally calculated nominal value over a specified range of the solution domain. The PIRTs used in the ESBWR TRACG application (Reference 7.10) for conservative cases are listed in Table 5-1. [[

]].

In addition to the parameters listed in Table 5-1, a 2σ uncertainty is also added to the decay heat in the conservative cases. This is accomplished through the decay heat input rather than a TRACG PIRT parameter; hence, this is not included in the PIRT. The delayed neutron effect is also included in the decay heat.

Table 5-1: TRACG PIRT Parameters Used in Mass and Energy Release Calculations

TRACG PIRT Parameter	Modeling Parameter	Standard deviation (σ)	ESBWR ECCS-LOCA	ESBWR Containment Mass and Energy Release	BWRX-300 Containment Mass and Energy Release
[[					
					]]

5.2.6 Initial Conditions for Base and Conservative Cases, Trips

The initial values used in the base and conservative cases are listed in Table 5-2. The trips and isolation signals used in pipe break cases are listed in Table 5-3.

Table 5-2: Initial Conditions Used in TRACG Mass and Energy Calculations

Parameter	Base Case Input	Conservative Case Input
Reactor power before shutdown	100% of rated power	102% of rated power
Feedwater temperature	Normal feedwater temperature	Reduced feedwater temperature for liquid break, normal feedwater temperature for steam break
Steam and feedwater flow rates	From heat balance at 100% of rated power	From heat balance at 102% of rated power
Dome pressure	Rated dome pressure	[[ ]] higher than rated dome pressure
Hot channel power shape	Obtained from core loading of a typical core design	Top peaked [[
Initial water level	Normal water level	]]

Table 5-3: Trips and Isolations Used in Both Base and Conservative Cases

Event or isolation	Trip	Notes
Shutdown	Load rejection (loss of offsite power)	Delay in generating the scram signal + time required for prompt neutron fission power to diminish because of the control rod insertion. Note that delayed neutron effect is accounted for in the decay heat separately.
Isolation of large pipes except IC piping	High drywell pressure or Low-Low level (Level 2)	These are the only RPV isolation signals credited in pipe break analyses.
Isolation of IC piping	[[	]]
Containment isolation	Same as RPV isolation valves	Containment isolation for main steam pipe break is conservatively ignored (see Section 3.0).
ICS Initiation	Low-low level (Level 2) or high drywell pressure	These are the only initiation signals for the ICS credited in the pipe break analyses.

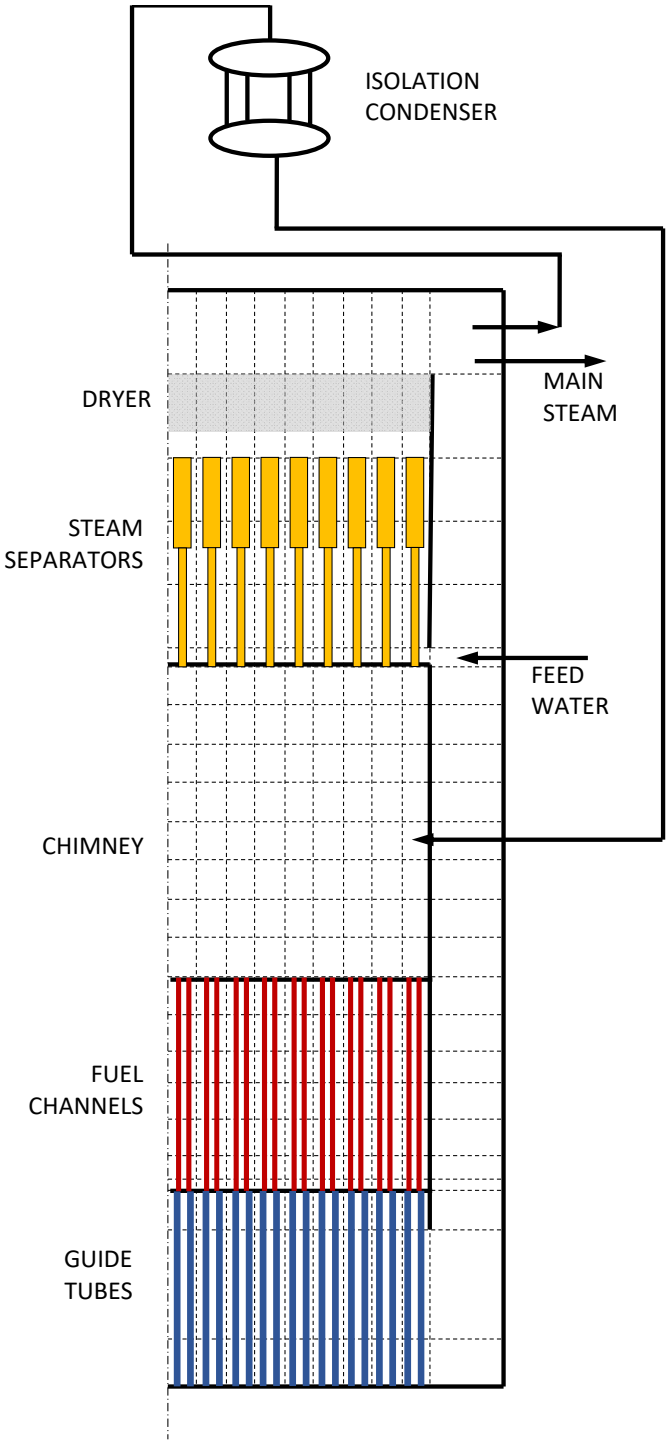

Figure 5-2: TRACG RPV Nodalization

[[

]]

Figure 5-3: Main Steam, Feedwater and Instrument Piping Attached to the RPV

[[

]]

Figure 5-4: TRACG IC Modeling for BWRX-300

5.3 Demonstration Cases for Large Breaks

The worst assumed single failure for a large break is the loss of an ICS train. [[

]]. For all other breaks, two ICS trains are available to remove the decay heat and depressurize the RPV after the loss of one ICS train due to a single failure. [[

]].

The demonstration cases for large steam and feedwater pipe breaks were performed for two sets of assumptions discussed below.

Base Case: Using nominal initial conditions and nominal modeling parameters. The nominal modeling parameters are used when all the PIRT multipliers described in Section 5.2.5 are set to 1.0. It should be noted that the base cases also include some conservatism due to the scenario and various input parameters. For example, [[

]].

Conservative Case: The initial conditions listed in Table 5-2 are biased and the modeling parameters listed in Table 5-1 are biased in the conservative direction.

The key input parameters used in the demonstration cases for base and conservative cases are collected in Table 5-4.

The scenario assumptions for main steam pipe break are as follows:

- Main steam pipe break inside the containment concurrent with loss of offsite power
- Feedwater pump trip [[ ]]
- Reactor trip [[

]].

- Drywell pressure increases to the high drywell pressure setpoint. [[

]].

- The ICS valves for one IC train begin opening [[
]].

Table 5-4: Key RPV Input Parameters Used in Demonstration Cases

Parameter	Base Case	Conservative Case
Initial power (MW)	870	887.4
Decay heat	ANS 5.1-1979 nominal	ANS 5.1-1979 + 2σ
Number of fuel bundles	240	240
Initial dome pressure (kPa)	[[	
Initial feedwater temperature (°C)		
Initial downcomer level (m above TAF)		
Main steam pipe inside diameter (m)		
Main steam flow limiter diameter (m)		
Feedwater pipe inside diameter (m)		
Low-low setpoint (m above TAF)		
High drywell pressure setpoint (kPa-g)		]]

5.3.1 Base Case for Large Feedwater and Steam Breaks

The large steam pipe breaks results are shown on Figure 5-5 through Figure 5-7. As discussed in Section 5.2.3, reactor power is obtained from decay heat tables.

The reactor power shown on Figure 5-5 is [[

]].

Only one ICS train is assumed to be put in service for large steam breaks. As the ICS condensate return valve starts opening at [[ ]], the cold condensate that has accumulated in the heat exchanger tubes and the condensate return lines starts flowing into the RPV, and a rush of steam to the ICS occurs. [[

]]. After this initial transient, the ICS heat removal rate starts approaching the 33.75 MW quasi steady state design value

As shown on Figure 5-6, the reactor pressure decreases for [[ ]] due to the break. [[ ]] the ICS starts depressurizing the RPV because the heat removal by one IC train exceeds the decay heat after approximately 20 seconds. [[

]].

The break flow rates from the broken loop and the intact loop sides of the break are shown on Figure 5-7. [[

]].

The large feedwater pipe break cases consider reduced feedwater temperature [[

]]. The results of the large feedwater pipe breaks are shown on Figure 5-8 through Figure 5-10.

In the steam pipe break cases, scram signal is inserted due to [[

]].

5.3.2 Conservative Case for Large Feedwater and Steam Breaks

The results of the large steam pipe breaks are shown on Figure 5-11 through Figure 5-13. The discussions in Section 5.3.1 for the base case also apply to the conservative case.

[[

]].

The results for the large feedwater pipe breaks are shown in Figure 5-15 through Figure 5-17. [[

]].

5.4 Demonstration Cases for Small Breaks

Base and conservative cases were run for the small steam and liquid pipe break cases. The small break events are slowly evolving events; therefore, the trends for the base and conservative steam and liquid breaks are very similar to each other. The results of the conservative small steam and liquid break cases are shown and discussed in this section.

The results of the conservative case for small break are shown on Figure 5-18 through Figure 5-22. As shown on Figure 5-18 and Figure 5-19, the ICS heat removal rate decreases as the RPV pressure decreases. The difference between the heat removed by the ICS and the power generated by decay heat is what is discharged from the break. The pressure boundary condition used in the TRACG calculation remains at atmospheric pressure to maximize the break flow rate. [[

]].

Even without crediting any inventory makeup, the downcomer level shown on Figure 5-20 remains above TAF out through 72 hours when the calculation ends for the conservative small steam break. As shown on Figure 5-21, the Peak Cladding Temperature (PCT) always remains only slightly above the fluid saturation temperature, [[

]]

As shown on Figure 5-22, at 72 hours after initiation of the small steam break, the break flow rate from the conservative case has reduced to well below the flow rate that can be made up with CRD flow.

Results from the conservative case for the small liquid breaks are shown on Figure 5-23 through Figure 5-27. There are differences from small steam break results in the break flow rate and RPV level while the break location is in the liquid space. Break uncovery starts to occur at [[ ]]. Because of the higher flow rate prior to the break uncovery and higher RPV inventory depletion as a result, downcomer level decreases [[ ]] as shown on Figure 5-25.

By 72 hours, downcomer [[

]].

At 72 hours after initiation of the small liquid break, the break flow rate from the conservative case has reduced [[ ]] as shown on Figure 5-27. This break flow at 72 hours corresponds roughly to the total steaming rate from decay heat minus the ICS steam condensation rate. The break flow at 72 hours is essentially the same as for the small steam break because the small liquid break became a small steam break when the break elevation uncovered [[ ]]. The break flow rate is well below the rate that can be made up with CRD flow.

5.5 Summary of the Application Method for Large and Small Break LOCA Analyses

The BWRX-300 TRACG nodalization for the RPV and ICS modeling is more detailed than the nodalization used in the ESBWR application discussed in Section 5.2.1.

The main steam piping of both loops up to the turbine stop valves are included in the model, and a large steam pipe break flow includes the flow from both ends of the break conservatively assuming instantaneous separation of the pipes.

Conservative biases listed in Table 5-1 are used to bound uncertainties in key TRACG models. For the conservative cases, the initial operating conditions are also conservatively biased as listed in Table 5-4.

Initiation of valve actuation timing used in the analysis bounds the time required to reach the analytical setpoint, signal development time, and the time required for valve stem travel until the area restriction starts to occur.

Reactor trip occurs due to load rejection in the small pipe break cases. RPV isolation valves are closed when the containment pressure exceeds the high containment pressure trip setpoint. The delay in this trip can be estimated conservatively.

[[

]]

[[

]]

Figure 5-5: Reactor Power, Main Steam Pipe Break, Base Case

Note: Decay Heat curve represents fission power as well as decay heat. "Q IC-A" is the heat removal rate by ICS Train A.

[[

]]

Figure 5-6: RPV Pressure, Main Steam Pipe Break, Base Case

[[

]]

Figure 5-7: Break Flow Rate and Enthalpy, Main Steam Pipe Break, Base Case

[[

]]

Figure 5-8: Reactor Power, Feedwater Pipe Break, Base Case

Note: Decay Heat curve represents fission power as well as decay heat. "Q IC-A" and "Q IC-B" are heat removal rates by ICS Trains A and B.

[[

]]

Figure 5-9: RPV Pressure, Feedwater Pipe Break, Base Case

[[

]]

Figure 5-10: Break Flow Rate and Enthalpy, Feedwater Pipe Break, Base Case

[[

]]

Figure 5-11: Reactor Power, Main Steam Pipe Break, Conservative Case

Note: Decay Heat curve represents fission power as well as decay heat. "Q IC-A" is the heat removal rate by ICS Train A.

[[

]]

Figure 5-12: RPV Pressure, Main Steam Pipe Break, Conservative Case

[[

]]

Figure 5-13: Break Flow Rate and Enthalpy, Main Steam Pipe Break, Conservative Case

[[

]]

Figure 5-14: RPV Level, Main Steam Pipe Break, Base and Conservative Cases

[[

]]

Figure 5-15: Reactor Power, Feedwater Pipe Break, Conservative Case

Note: Decay Heat curve represents fission power as well as decay heat. "Q IC-A" and "Q IC-B" are the heat removal rates by ICS Train A and ICS Train B.

[[

]]

Figure 5-16: RPV Pressure, Feedwater Pipe Break, Conservative Case

[[

]]

Figure 5-17: Break Flow Rate and Enthalpy, Feedwater Pipe Break, Conservative Case

[[

]]

Figure 5-18: Power, Small Steam Break, 2 ICS Trains, Conservative Case

Note: Decay Heat curve represents fission power as well as decay heat. "Q IC-A" and "Q IC-B" are heat removal rates by ICS Trains A and B.

[[

]]

Figure 5-19: RPV Pressure, Small Steam Break, 2 ICS Trains, Conservative Case

[[

]]

Figure 5-20: RPV Level, Small Steam Break, 2 ICS Trains, Conservative Case

[[

]]

Figure 5-21: PCT, Small Steam Break, 2 ICS Trains, Conservative Case

[[

]]

Figure 5-22: Break Flow Rate and Enthalpy, Small Steam Break, 2 ICS Trains, Conservative Case

Note: The initial break flow rate is off-scale. [[
]]

[[

]]

Figure 5-23: Power, Small Liquid Break, 2 ICS Trains, Conservative Case

Note: Decay Heat curve represents fission power as well as decay heat. "Q IC-A" and "Q IC-B" are heat removal rates by ICS Trains A and B.

[[

]]

Figure 5-24: RPV Pressure, Small Liquid Break, 2 ICS Trains, Conservative Case

[[

]]

Figure 5-25: RPV Level, Small Liquid Break, 2 ICS Trains, Conservative Case

[[

]]

Figure 5-26: PCT, Small Liquid Break, 2 ICS Trains, Conservative Case

[[

]]

Figure 5-27: Break Flow Rate and Enthalpy, Small Liquid Break, 2 ICS Trains, Conservative Case

6.0 CONTAINMENT ANALYSIS METHOD USING GOTHIC

The GOTHIC application methodology includes base cases and conservative cases. For the base cases, nominal inputs, assumptions, and correlations are used. The individual key inputs, assumptions and modeling parameters are conservatively biased simultaneously in the conservative cases, rather than sampling the uncertainties and adding margin to the base case results. While this method compounds conservatisms, it gives reasonable assurance that the overall method results bound the uncertainties, and greatly reduces the number of sensitivity runs. This is the same approach that was taken for the ESBWR containment method in Reference 7.10.

Sections 6.1 through 6.4 describe the identification of the relevant inputs and phenomena relevant to the BWRX-300 containment response and the selection of the models and correlations used to develop the base GOTHIC containment model. Section 6.5 describes the GOTHIC input model for the BWRX-300 containment. Section 6.6 describes the base cases and the results obtained from those base cases. Section 6.7 shows how nodalization impacts the calculated results. Sections 6.5 through 6.7 help to establish what model uncertainties and biases of the GOTHIC methodology are most important for application of the GOTHIC model for analyses of the BWRX-300 containment; that is why Sections 6.5 through 6.7 are presented before the discussion of the model biases and uncertainties in Section 6.8. Section 6.8 reviews the key model uncertainties and biases used in developing the conservative GOTHIC containment model. Section 6.9 provides benchmark predictions of test data. Demonstration analyses showing the BWRX-300 containment response for various break sizes and locations using the conservative GOTHIC containment model are provided in Section 6.10.

The large steam line break result described in Section 6.10.1 produces the highest calculated containment pressure. Containment pressure and temperature responses calculated using the conservative case assumptions are compared to the base case results to quantify the amount of conservatism provided by the methodology.

The small steam or liquid breaks described in Section 6.10.2 demonstrate that the peak containment pressures from unisolated small breaks are well below the peak pressure resulting from the large steam break. The small break calculations are primarily useful for demonstrating the capability of the PCCS to reduce the containment pressure in the longer term. The methodology assumes a one-way coupling between the TRACG and GOTHIC calculations whereby atmospheric pressure is always used for the break boundary condition used to calculate conservative TRACG mass and energy release rates that are input to the GOTHIC containment calculation. This methodology is demonstrated in Section 6.10.2 to result in peak containment pressures from the small breaks that are greater or more conservative than what would be obtained if a more complex two-way coupled methodology that credits how increased containment pressure were used. After the containment pressure increases to the RPV pressure, the RPV pressure calculated without a break bounds the containment pressure.

6.1 GOTHIC Phenomenon Identification and Ranking Table (PIRT)

The PIRT purpose is to identify phenomena important to the analysis of the BWRX-300 containment response for design basis events. The phenomena is then used to assess the ability of the model to calculate the effect of the phenomena on containment pressure and temperature, and the qualification of the evaluation model for calculating the phenomena, including the available

tests and determining any additional testing, scaling or analysis needed to qualify GOTHIC for the BWRX-300.

The initial phenomena list relevant to BWRX-300 containment analysis has been obtained by reviewing the following sources:

- NEDC-33083P-A Revision 1, TRACG Application for ESBWR (Reference 7.10)
- NEA/CSNI/R3(2014), Containment Code Validation Matrix (Reference 7.13)
- SMSAB-02-02, An Assessment of CONTAIN 2.0: A Focus on Containment Thermal Hydraulics (Including Hydrogen Distributions) (Reference 7.14)

Table 3.2-1 of Reference 7.10 was reviewed for phenomena that are applicable to the BWRX-300 containment pressure and temperature analysis, including phenomena that would have an equivalent phenomena in BWRX-300, even if the component was of a different design (for example, the secondary side heat transfer to the ultimate sink pools was evaluated because the phenomena are equivalent for the [[ ]]).

Two additional references (References 7.13 and 7.14) were used for additional important phenomena that might apply to the BWRX-300, but not to the ESBWR. This provides a complete check that covers phenomena that were not determined important for ESBWR but might be important for the BWRX-300. Table 3-1, *Containment Thermal Hydraulics Phenomena*, and Table 3-6, *Systems Phenomena*, of Reference 7.13 were reviewed. Note that the phenomena applicable only to the beyond design basis events and severe accidents are not included in the review. Reference 7.13 report classifies the significance of phenomena as Major/Minor. Phenomena evaluated as having major significance were reviewed for BWRX-300 applicability. The phenomena were then correlated with the ESBWR PIRT to eliminate duplication.

The third reference (Reference 7.14) contains Table 2.3, *Illustrative Phenomena Identification and Ranking Table for Containment Thermal Hydraulics*, during the Rapid Pressurization Phase of a Design Basis Accident in a Large Dry Pressurized Water Reactor Containment. This Table repeats the same phenomenon in different structures/components of the containment, but if the phenomenon was ranked H, M or L-M for either Pressure or Temperature, it was evaluated for correlation with the phenomenon in the previous two sources. Note that fan dynamics, spray dynamics and spray mass and energy exchange are not applicable to BWRX-300 and are not evaluated. All the buoyancy phenomena in Reference 7.14 are combined into one buoyancy phenomena, and the convection/advection phenomena are combined. The phenomena in Reference 7.14 report phenomena are then correlated with the ESBWR PIRT to eliminate duplication.

The names of phenomena are different in the reports cited above, although they refer to the same phenomena. For the BWRX-300 containment PIRT, the phenomena names and descriptions provided in Reference 7.10 were generally used.

6.2 PIRT Survey

The initial list of PIRTs was distributed in a survey to six Subject Matter Experts who reviewed the PIRT list, ranked them in importance to the GOTHIC BWRX-300 containment pressure and temperature analysis, and solicited any missing significant phenomena. The experts were provided with the BWRX-300 design description, including the information in Section 3.0 discussed previously. Phenomena ranking was requested according to the criteria in Table 6-1.

Table 6-1: Phenomena Ranking Criteria

Importance	Definition
High (H)	Phenomenon has controlling effect on GOTHIC DBA LOCA Containment Pressure and Temperature
Medium (M)	Phenomenon has moderate effect on GOTHIC DBA LOCA Containment Pressure and Temperature
Low (L)	Phenomenon has low effect on GOTHIC DBA LOCA Containment Pressure and Temperature
Not Applicable / Not Relevant (N/A)	Phenomenon has no, or insignificant effect on GOTHIC DBA LOCA Containment Pressure and Temperature for the design basis events described in Section 1.2. This category also applies to phenomena that are only significant to TRACG DBA LOCA mass and energy release

To facilitate downstream application to the GOTHIC methodology qualification, the rankings were broken down into two phases:

1. Short-term is the period during which the momentum and inertia effects resulting from the break flow have a significant contribution to the circulation, stratification and heat tranfer in the containment. [[

]]

2. Long-term is the period during which the momentum and inertia effects are diminished, and the buoyancy is the major contributor to the circulation, stratification and heat transfer. This phase may be as long as 30 days, but the calculations are continued only until conditions are considered stable.

The experts were asked to evaluate the Systems Structures and Components (SSCs) involved in GOTHIC modeling of the BWRX-300 containment in their ranking and provide a single highest importance rank for the phenomena. Similarly, if the phenomena might have different rankings between a liquid pipe break and a steam pipe break, they were asked to provide the higher/bounding rank, to make the presentation of the ranking simpler and the ranking/consensus building process more efficient.

The surveys were provided for expert's comments and additional input on the applicable SSCs. They were encouraged to: "Use the comments column if meaning of the phenomena are unclear." Blank fields were provided to add any missing phenomena thought to be significant.

Before the survey was completed, a "Pre-job brief" meeting was held to explain the process and answer general questions.

In consolidating the survey results, comments on the description/definition of the phenomena were identified. A few additional phenomena were identified by the experts during the survey. Additional input was obtained with clarified definitions and with ranking of the added phenomena.

After the initial survey was received and compiled, multiple meetings were held to discuss the results and develop a consensus ranking. These discussions focused on phenomena with the highest variance in the ranking. Explanation of the rationale for an individual's ranking usually resulted in changes to the ranking and built a consensus ranking.

The High/Medium/Low/N/A ranking was assigned a numerical score of 3/2/1/0, respectively. The rank was then averaged and rounded up (if the average is 2.5 or greater it is assigned a H/High importance, and if it is less than that and above 1.5 it is assigned a M/Medium importance).

It should be noted that the ranking was completed before performing sensitivity studies and before the preliminary best estimate calculations were progressed. Therefore, the rankings reflect phenomena that may potentially be applicable. In this context, the rankings can be viewed as a conservative estimate such that a phenomenon will be included in the uncertainty evaluations if there is a potential for it to affect the calculations. A phenomenon ranked medium or high may turn out to be not applicable or of low effect when the calculations are performed. But the opposite would not be the case (i.e., phenomena ranked low following the consensus ranking process were not revisited).

The summary of the PIRT is provided in Table 6-2. A description of each phenomena is given below the Table corresponding to the item number in Table 6-2.

Table 6-2: Phenomena Identification and Ranking Table for Containment (Excluding RPV)

[[

]]

6.3 Overview of the Development of Assessment Base

Development of the assessment base follows the applicable sections of RG 1.203 guidance. It should be noted that most Elements 2 and 3 in RG 1.203 have been completed as part of the GOTHIC code development and documented in the GOTHIC technical and qualification reports. The remaining items of RG 1.203 Elements 2 and 3 include:

- Determining uncertainty in the correlations relating to the phenomena ranked high and medium based upon the existing experimental base for these correlations
- Establishing suitably conservative biases in the above correlations
- Establishing suitably conservative input parameters
- Benchmarking the method against the integral tests representative of the BWRX-300 containment to demonstrate the conservatism in the method

6.4 Knowledge Level for the Phenomena Pertinent to Containment Analysis

The phenomena that are ranked High or Medium for either short or long-term are included in the uncertainty evaluation. The first step in this process is to assess the knowledge level for each of these phenomena. The same expert panel that formed the PIRT in Table 6-2, with one substitute due to the departure of one member from GEH, also voted on the knowledge level in Table 6-3. The knowledge level is ranked from 1 to 4 for each phenomenon, 1 representing the least confidence and 4 representing the most confidence. The consolidated rationale for the knowledge level is also listed in Table 6-3.

In general, a phenomenon ranked high in Table 6-2 for importance and low in Table 6-3 for knowledge level requires additional research. However, some of the phenomena ranked High or Medium importance may not be applicable or the effect may turn out to be small for the type of modeling and the analysis of the events that are in the scope of this report as mentioned in Section 6.3. It is for this reason that the base GOTHIC model and the base case results will be introduced in the next section before discussing the uncertainties in the inputs and correlations.

Table 6-3: Knowledge Level for the Phenomena Ranked High or Medium

[[

]]

6.5 GOTHIC Containment Model

A schematic of the GOTHIC model used for the BWRX-300 containment analysis is shown on Figure 6-1. Volume 1s represents the main section of the containment, Volume 2s represents the containment dome region above the refueling bellows, Volume 3s is the PCCS, and Volume 4 is the reactor cavity pool.

The containment dome is connected to the main section of the containment through two flow paths, 1 and 2, representing the manholes in the refueling bellows.

Flow paths 4 through 13 are the exit of the hot channels of the [[ ]] PCCS units connected to the reactor cavity. Flow paths 14 through 23 are the intake openings of the PCCS units connected to the reactor cavity pool. Flow paths 25 through 34 are openings between the cold tubes and heated tubes of the PCCS units at the bottom.

Three dimensional volumes, so-called subdivided volumes in GOTHIC terminology, are used to model the main section of containment. Nodalization of the main section (Volume 1s) and the containment dome (Volume 2s) used in the base model are shown on Figure 6-2.

The RPV is modeled by using a blockage corresponding to the outer dimensions of the RPV insulation as shown on Figure 6-2. Approximately [[ ]] of the remaining volume is assumed to be obstructed by various support structures, piping, catwalks, etc. Thermal conductors are distributed over cells on the RPV surfaces and where the piping is routed. The thermal conductor properties are set to the mirror insulation properties using conservative inputs to maximize the heat loads from the RPV and piping. The fluid temperature in the piping is assumed to be the same as the RPV fluid temperature and is specified as a function of time as obtained from the TRACG mass and energy release calculations.

The flow path representing the break flow is placed [[ ]], next to the containment shell and the break flow is directed toward the shell when calculating the peak shell temperature. [[

]] The break mass flow rate and enthalpy are specified as a function of time as obtained from the TRACG mass and energy release calculation.

The figures based on the GOTHIC runs with break location maximizing the pressure are identified with “[MaxP]”, and the figures based on the GOTHIC runs with break location maximizing the shell temperature are identified with “[MaxT]” in the figure captions.

Nodalization for the small containment dome region is shown in the upper right part of Figure 6-2. [[

]]

The PCCS is represented by subdivided volumes as shown on Figure 6-3. [[

]]

The following is a list of the key modeling parameters used in the base cases. The reasoning for the choice of the models and their uncertainties is discussed in Section 6.8.

- Mass and energy release are obtained from the TRACG base case results in Section 5.3.1 for large breaks.
- The form loss coefficients in the PCCS are set to conservatively high values, accounting for the flow losses due to the typical spacers, as well as entrance and exit losses and [[ ]].
- Wall friction is calculated from the Colebrook relationship for smooth wall.
- The heat transfer coefficient in containment is the sum of two parts as follows:
    - The Nusselt number for heat transfer due to sensible heat can be calculated from the forced convection or natural convection. The forced flow convection correlation is the Dittus-Boelter correlation given by:

      $$Nu_{FC} = 0.023\,\mathrm{Re}^{0.8}\,\mathrm{Pr}^{0.3}$$

      where Nu is the Nusselt number, Re is the Reynolds number, and Pr is the Prandtl number. Reynolds number is calculated based on the velocity and properties in the node next to the wall and the user-specified characteristic length. The exponent of the Prandtl number is 0.4 for the heated walls (RPV and hot piping).

      The Nu for heat transfer in natural convection is calculated from the [[

]]

The following relationship is used in GOTHIC to select which mode of heat transfer applies:

[[ ]]

- Heat transfer due to latent heat in condensation is calculated using the Diffusion Layer Model (DLM) (Section 9.1.6 of Reference 7.16).

- The characteristic length for the forced convection is set to the [[ ]].
- Radiation heat transfer to the shell and the PCCS is conservatively ignored.
- [[

]]

[[

]]

Figure 6-1: Schematic of the GOTHIC Model of BWRX-300 Containment

[[

]]

Figure 6-2: Nodalization of Containment Main Volume, Volume 1s (left), Containment Dome, Volume 2s, (upper right) and the Break Flow Path in Volume 1s at Vertical Node 14 (lower right) [MaxT]

[[

]]

Figure 6-3: Volumes Representing PCCS Units

6.6 Base Cases and Results

This section presents the containment response for the mass and energy releases calculated in Section 5.3.1 for large steam and feedwater breaks using the base model described in Section 6.5. The key containment inputs are listed in Table 6-4. The containment nodalization and modeling parameters are described in Section 6.5.

Table 6-4: Containment Inputs Used in Base Cases

Parameter	Value
Containment height	[[
Containment diameter	
Free containment volume (excluding dome)	
Containment dome height	
Containment dome diameter	
Containment shell thickness	
Containment head thickness	
Number of manholes on the refueling bellows	
Diameter of the manholes	
Number of PCCS units	
PCCS type	
PCCS outer diameter	
PCCS outer pipe thickness	
PCCS cold tube outer diameter	
PCCS cold tube thickness	
PCCS height inside the containment	]]
Initial containment temperature	43.33 °C
Initial containment relative humidity	20%
Initial containment pressure	101.325 kPa
Initial reactor cavity pool temperature	43.33 °C

6.6.1 Containment Response to Large Steam Break, Base Case

The containment pressure response to a large break in a steam line is shown on Figure 6-4. The peak pressure [[ ]] is reached at approximately the time the RPV isolation valves fully close at ten seconds. After the closure of the RPV isolation valves, the only heat input to the containment is due to convection from the RPV wall and hot pipe walls through the insulation. With the break flow isolated, the containment pressure starts decreasing. [[

]]

The airspace and containment shell temperature responses are shown on Figure 6-5. The maximum air temperature is the maximum of all nodal temperatures in the containment; the bulk temperature is the average air temperature throughout the containment. These temperatures are higher than the temperature resulting from the isenthalpic expansion of steam from the RPV conditions to the containment pressure. The additional temperature increase is due to the compression of nitrogen in containment. Following the break, there is a rigorous circulation of

the air in containment. Prior to isolation, the [[

]]. The peak temperature moves around in containment as the hot steam / nitrogen mixture circulates. After the break flow stops, the location of the maximum temperature continues to vary with the changing flow patterns, but most of the time remains in locations near the RPV wall.

Although the containment air temperature is high [[ ]], the containment shell remains at a much lower temperature. [[

]]

The PCCS exit temperature is also shown on Figure 6-5. [[

]] A sensitivity analysis for the PCCS is presented in Section 6.6.1.

The decay heat rate and the heat removal rates by the various heat removal mechanisms are plotted on Figure 6-6. As shown on the plot, the containment shell initially absorbs a large amount of energy for a short duration before the heat removal diminishes as the shell warms up [[ ]]. The isolation condensers are the primary mechanism for removing decay heat from the isolated RPV. [[

]] No credit is taken in these cases for the heat transfer from the containment shell to the concrete supporting structures.

The subcompartment formed by the containment head and refueling bellows is the limiting location with respect to differential pressures acting across subcompartment boundaries because of the relatively small flow areas provided by the access manholes in the bellows. The other subcompartments inside the containment (e.g., [[ ]]) have much larger openings. The pressure differential across the refueling bellows is shown on Figure 6-8. In this variation of the base case, the flow loss coefficient across the manholes is set to an extremely high value [[ ]] in order to maximize the differential pressure during the event. The GOTHIC model captures the pressure waves travelling through the containment immediately following the break, and the peaks and valleys in the pressure trend correspond to physical phenomena. The time

difference between the first peaks of the red and blue curves is consistent with the pressure wave travelling at nearly the speed of sound. [[
]]. This is a small pressure differential across the boundary of a subcompartment. The pressure drop across the other subcompartment boundaries were not calculated because they have much larger flow area-to-volume ratios and are located farther away from the break, [[
]].

If the pipe routing is designed such that a potential pipe break may occur in close proximity of the biological shield wall or vessel support, the same method used here can be used to assess the differential pressure loads to be considered in the detailed structural designs. However, if a significant pressure differential occurs across the biological shield due to the close proximity of the break, it is likely that the jet impingement loads would be the more limiting concern. The determination of the jet impingement loads acting on the containment structures is outside the scope of this LTR.

6.6.2 Containment Response to Large Feedwater Pipe Break, Base Case

The containment pressure response to a large break in the feedwater pipe is shown on Figure 6-9. The peak pressure [[ ]] is reached at the time the RPV isolation valves fully close [[ ]]. Similar to the large steam break, after the closure of the RPV isolation valves the only heat input to the containment is from the RPV wall and hot pipe walls through the insulation. [[ ]] The peak containment pressure for a feedwater pipe break is bounded by the peak containment pressure for a large steam pipe break.

The airspace and containment shell temperature responses in the containment are shown on Figure 6-10. The containment temperature discussion in Section 6.6.1 also apply to the response to feedwater pipe breaks. It can be seen on Figure 6-10 that the maximum shell temperature is well below the containment atmosphere temperature, [[
]].

6.7 Nodalization Studies

6.7.1 Nodalization Study for Containment

A nodalization study was performed using the base case for the large main steam pipe break presented in Section 6.6.1.

The nodalization study for the main containment section included the following cases, also shown on Figure 6-11:

- Base case: [[ ]]
- Coarser grid. Twice the node size of the base case in each direction: [[ ]]
- Finer grid in the horizonal plane. Half the node size of the base case in each direction in the horizontal plane: [[ ]]. Same node size in the vertical direction
- Finer grid in the vertical direction: Half the node size of the base case in the vertical direction: [[ ]]. Same node size as in the base case in the horizontal plane

The PCCS unit placement is accurate in the [[ ]] cases. [[ ]].

The large steam break base case was rerun using different nodalization schemes described above. As shown on Figure 6-12, the effect of nodalization on the containment pressure response is very small. The curve for [[ ]] case is not visible because it is overlapped by the results of the [[ ]] nodalization case. There is an insignificant difference, [[ ]], in the peak pressure between the base case and finer nodalization cases. The nodalization trend also shows that the coarser nodalization slightly overpredicts the peak pressure. As shown on this figure, reducing the node size [[ ]] does not make a significant difference in the pressure response.

The temperature trends shown on Figure 6-13 also display similar behaviors. The air/steam mixture temperatures are similar in all cases. The temperature trend differences between the cases are consistent with the differences shown between the pressure trends. There are some differences in the air/steam temperatures in the longer term, but the shell temperatures remain close to each other in all nodalization schemes. [[ ]].

Based on the above results, it is concluded that the containment nodalization [[ ]] is adequate for containment pressure, air/steam temperature and the shell temperature predictions.

6.7.2 Nodalization Study for PCCS

The effect of nodalization on the PCCS has been studied for a single PCCS unit placed in a large containment volume. The containment volume is kept at the prescribed temperature and steam concentration. The base case nodalization in the vertical direction is the same as the BWRX-300 containment model, [[

]]

The second case used in the nodalization study doubles the number of nodes both in the PCCS and the containment, and the third case doubles the number of nodes again.

The effect of nodalization on the heat removal rate is shown on Figure 6-14 at three containment temperatures. [[

]] A [[ ]] reduction is applied to the heat transfer on the outer surface of the PCCS unit. [[ ]] The results show negligible effect of nodalization on the PCCS heat removal rate.

[[

]]

Figure 6-4: Containment Pressure Following Large Main Steam Pipe Break, Base Case [MaxP]

[[

]]

Figure 6-5: Temperatures in the Containment Following a Large Main Steam Pipe Break, Base Case [MaxT]

[[

]]

Figure 6-6: Heat Removal Rates by Various Mechanisms Following Large Main Steam Pipe Break, Base Case [MaxP]

[[

]]

Figure 6-7: Longer Term Heat Removal Rates by Various Mechanisms Following Large Main Steam Pipe Break, Base Case [MaxP]

[[

]]

Figure 6-8: Pressures Next to Refueling Bellows Following Large Main Steam Pipe Break, Base Case [MaxT]

[[

]]

Figure 6-9: Containment Pressure Following Large Feedwater Pipe Break, Base Case [MaxP]

[[

]]

Figure 6-10: Temperatures in the Containment Following a Large Feedwater Pipe Break, Base Case [MaxT]

[[

]]

Figure 6-11: Grid Used in Nodalization Studies [MaxP]

Note: Orange circles in the plan view and orange bars in the vertical view represent the PCCS units. Blue arrows represent the break locations. In the vertical view, the break location arrows indicate only the vertical node number. The break location is shown for the cases maximizing temperature. In the cases maximizing pressure, the break flow is directed upwards, in cell IX=12, IY=6, IZ=10 in the 16x16x16 case, and in the corresponding cells in the other cases.

[[

]]

Figure 6-12: Effect of Nodalization on the Containment Pressure Response to Large Steam Pipe Break, Base Case [MaxP]

[[

]]

Figure 6-13: Effect of Nodalization on the Containment Temperature Response to Large Steam Pipe Break, Base Case [MaxT]

[[

]]

Figure 6-14: Effect of Nodalization on the PCCS Heat Removal Rate

6.8 Model Uncertainties and Biases

The source of uncertainties in the phenomena important to the containment pressure and temperature response are identified in Section 6.2. The knowledge level for these phenomena is discussed in Section 6.4 and summarized in Table 6-3. The following is the grouping of phenomena and their assessment based on the observations from the results of the base case containment analysis discussed in Section 6.6.

- [[

]]

- Items 2, 5, 6, 11, 12 are inputs. [[

]].

- The natural and forced circulation and stratification are affected by the friction factors, turbulence modeling, and the model nodalization. A nodalization study is presented in Section 6.7 for the containment and the PCCS. A sensitivity study for the friction factors and turbulence modeling is presented in Section 6.8.1 [[ ]]. This addresses Items 9, 10, 13, and 14.
- Uncertainties in the convection and condensation heat transfer coefficients, Items 3 and 7, are discussed in Section 6.8.2 where bounding values have been developed.
- In the RPV the production of hydrogen and oxygen by radiolysis is modeled by the bounding correlation given in Section 5.2.4. There are no other mechanisms for producing significant amounts of NC gases in either the RPV or the containment. [[ ]]. This addresses Items 19 and 20.
- Multi-component gas properties are calculated using the most accurate models available in the GOTHIC code as described in Reference 7.16.

6.8.1 Effect of the Friction Factors and Turbulence Parameters on the Containment Response

The importance of friction factors and turbulence on containment pressure and temperature response has been investigated by sensitivity studies for the containment and the PCCS separately.

The nominal cases use Colbrook's friction factors for a smooth surface. To determine the sensitivity of the pressure and temperature to the friction factor, the relative roughness was increased [[ ]]. Given the large hydraulic diameter, this relative roughness corresponds to an unreasonably high absolute value of surface roughness [[ ]]. The increased surface roughness case is identified as the "High C_f" case in the comparisons.

[[

]]

The results obtained by the above sensitivity cases are compared on Figure 6-15 through Figure 6-17 for the large steam pipe break. [[

]]

[[

]]

Figure 6-15: Effect of Friction and Turbulence on Containment Pressure, Large Steam Pipe Break [MaxP]

[[

]]

Figure 6-16: Effect of Friction and Turbulence on Containment Temperatures, Large Steam Pipe Break [MaxT]

[[

]]

Figure 6-17: Effect of Friction and Turbulence on Steam Volume Fraction, Large Steam Pipe Break [MaxT]

6.8.2 Uncertainties in the Convection and Condensation Heat Transfer Coefficient and the Bounding Values

The BWRX-300 containment model uses the DLM option for condensation built into GOTHIC (Reference 7.16) to calculate the condensation rate. The DLM correlation is based on a mechanistic model which recognizes the similarity between the heat and mass transfer. The benchmarking of both the convection and condensation correlations to the data is also provided in Reference 7.18. DLM is selected over the other options available in the code due to its mechanistic nature representing the underlying phenomena as opposed to curve fit to data. Recently, Heat and Mass Transfer Analogy Method (HMTAM) has been developed and compared to the CONAN and COPAIN test data (References 7.19 and 7.20). HMTAM is also based on the analogy between heat and mass transfer and is similar to DLM. As will be shown, the DLM method is more conservative than the HMTAM method for the BWRX-300 containment application. The uncertainties in the convection and condensation correlations with respect to the data will be evaluated based on the COPAIN test data in Reference 7.19. The uncertainties will be first presented for the HMTAM method.

The total heat transfer to a condensing surface has two parts: convection heat transfer from bulk to liquid film and the heat transfer by condensation. [[

]]

COPAIN data is collected over a range of 1 to 6.7 bars, non-condensable gas mass fraction range of 0.1 to 1.0, velocity range of 0.1 to 3.0 m/s and steam superheating up to 40 °C. The range of parameters in the BWRX-300 containment response is within the COPAIN data range. The COPAIN data also includes pure convection measurements. More information on the COPAIN data can be found in Reference 7.19.

A comparison of the forced and natural convection correlations to the data is shown on Figure 6-18. The black markers are the ratio of forced convection measured Nusselt number divided by the Nu number predicted by the Schlichting forced convection correlation. The points larger than 1.0 indicate that correlation underpredicts the forced convection Nusselt number. The x-axis in the plot is the Richardson number, Ri. Theoretically, inertia forces are dominant when the Richardson number is less than 1, and buoyancy forces are dominant when the Richardson number is greater than 1. As expected, the black markers corresponding to the Richardson numbers greater than about 5 show that the data is grossly underpredicted if the forced convection correlation is used where buoyancy forces are important. Conversely, the red markers, which show the ratio of the measured Nusselt number to the Nusselt number predicted by the McAdams natural convection correlation show that the data is grossly underpredicted if the natural convection heat transfer coefficient is used where the buoyancy forces are overwhelmed by the inertia forces due to the free stream velocity, i.e., where forced convection correlation should be used. There is a transition region between the high and low Richardson number ranges that is reviewed in more detail below.

The heat transfer is enhanced by the turbulence near the wall. As the free stream velocity is increased from zero in the same direction as in flow driven by buoyancy near the wall, it suppresses the turbulence and reduces the heat transfer until the free stream velocity is increased large enough that the inertial forces overwhelm the buoyancy forces. This phenomenon may occur in the transition region from natural convection to forced convection and is called re-laminarization. [[

]] Re-laminarization does not occur if the free stream flow is in upward direction near a cold wall as explained in Reference 7.21 and shown on Figure 6-19.

The analogy between the condensation and convection has been shown to be a valid basis to predict condensation in the more recent research and supported by data (see References 7.18 and 7.19). In condensation, the correlation forms and coefficients for forced and natural convection remain the same as in convection, but the Prandtl (Pr) number is replaced by the Schmidt (Sc) number, and the Nusselt (Nu) number is replaced by the Sherwood (Sh) number. The definitions of the dimensionless numbers are found in Reference 7.19.

[[
]] The uncertainty bands are shown on Figure 6-20 for forced and natural convection as compared to the data. [[

]] This is discussed further in the following application to BWRX-300 containment.

The discussion above is presented as it pertains to the HMTAM model of condensation, using Schlichting correlation for forced convection and McAdams correlation for natural convection.

The BWRX-300 containment model uses the DLM condensation model, [[
]].

The ratio of the condensation heat transfer predicted by DLM to that of HMTAM is shown on Figure 6-21 for various wall temperatures, flow rates and mass fractions. [[

]]

Based on the above observations, the following are the minimum biases applied to the DLM and convection correlations used in the GOTHIC model of the BWRX-300 containment to ensure the calculated results are conservative.

Convection correlation bias:

- [[

]]

Condensation correlation bias:

- [[

]]

[[

]]

As will be shown in Section 6.9, the above biases bound the integral test data and also add conservatism to the BWRX-300 containment response results that is comparable to the conservatism that would be introduced by using the Uchida correlation. Comparisons of the BWRX-300 containment response predicted by the Uchida correlation and the biased DLM correlation will be presented in Section 6.10.1.

[[

]]

[[

]]

Figure 6-18: Comparison of Data and Convection Correlations

[[

]]

Figure 6-19: Non-Dimensional Heat Transfer Coefficient Obtained With a Heated Tube in Upward Flow Conditions (from Reference 7.21)

[[

]]

Figure 6-20: Non-Dimensional Sherwood Number Obtained in the COPAIN Facility (Reference 7.19) With the Proposed Uncertainty Bands Added

[[

]]

Figure 6-21: Ratio of Condensation Mass Flow Rate Obtained by DLM to that of HMTAM

6.8.3 Sensitivity Analyses for PCCS Performance

Sensitivity analyses have been performed for the PCCS performance to determine the effect of:

- PCCS loss coefficients
- PCCS liquid-side heat transfer coefficient
- Fouling

Sensitivity cases also include the potential for the onset of boiling.

To determine the effect of each parameter without interference from other phenomena, a single PCCS unit was placed in a large volume representing a section of the containment. The containment pressure, temperature and steam volume fraction were kept constant at various values and each of the sensitivity parameters were varied to determine the effect on PCCS performance. The PCCS nodalization and geometry are the same as those used in the BWRX-300 containment model described in Section 6.5. The volume representing the containment was also nodalized in the vertical direction that is the same as the containment nodalization described in Section 6.5, with the exception of using one node in the horizontal direction.

The sensitivity study was performed for the following conditions. The PCCS heat removal rate at each condition was obtained after a steady state was reached.

Containment pressure: [[ ]]

Containment temperature: [[ ]]

Steam volume fraction: [[ ]]

PCCS inlet temperature: [[ ]]

PCCS total loss coefficient: [[ ]]

[[

]] The base case has no fouling or no paint.

The sensitivity cases for paint and crud assume thermal resistance of the paint on the outer surface of the PCCS is [[ ]] and the thermal resistance of the crud on the inner surface is [[ ]].

The results of the sensitivity cases are summarized in Table 6-5. [[

]]

Table 6-5: Summary of the Sensitivity Study Results for PCCS

Containment pressure (kPa)	[[					
Containment temperature (°C)						
Heat removal rate (kW)						
Loss coefficient x 1.5						
Loss coefficient x 2.0						
Fouling + paint						
Heat transfer coefficient inside the PCCS is reduced by [[ ]]						]]

6.9 Benchmarking to the Carolina Virginia Tube Reactor (CVTR) Integral Tests

The CVTR tests simulate a steam pipe break by injecting slightly superheated steam into a closed containment (Reference 7.22). CVTR has a dry containment, with a free volume of 6428 m^3 (227,000 ft^3), [[ ]]. The

walls are concrete with a 6.35 millimeter (1/4 inch) thick steel liner, [[
]].

The CVTR test has several cases [[ ]]. Test case #3 is relevant to the BWRX-300 containment benchmarking [[

]] The GOTHIC model for CVTR is shown on Figure 6-22.

As discussed in Reference 7.17, the three-dimensional GOTHIC model using the best estimate DLM, including the Film Enhancement condensation heat transfer, predicts the measured pressure and thermal stratification closely. In the "biased DLM" cases presented here, the DLM method is used without the Film Enhancement feature and the biases in Section 6.8.2 are applied to the heat transfer surfaces. The comparisons also include the pressure and temperature predicted by the Uchida correlation. Uchida condensation correlation does not include a bias. However, the same bias described in Section 6.8.2 is also applied to the convection heat transfer in the Uchida correlation cases.

Figure 6-23 shows the containment pressure benchmarking to test data. The peak pressure calculated by the biased DLM heat transfer coefficient is approximately [[ ]] higher than the data. The biased DLM case also bounds the pressure predicted by the Uchida correlation.

Figure 6-24 shows the airspace temperature and Figure 6-25 shows the structure surface temperatures. The calculated temperatures are higher than the measured temperatures. The differences in the calculated temperatures on Figure 6-24 and Figure 6-25 at higher and lower elevations are close to the differences in the measured temperatures. These results indicate that GOTHIC predicts stratification well while there is steam flow and after the steam flow stops. The predicted surface temperatures are higher than the data.

[[

]]

Figure 6-22: CVTR Facility (Reference 7.22) and the GOTHIC Model (Reference 7.17)

[[

]]

Figure 6-23: GOTHIC Benchmarking to CVTR Test Data, Containment Pressure

[[

]]

Figure 6-24: GOTHIC Benchmarking to CVTR Test Data, Airspace Temperature

[[

]]

Figure 6-25: GOTHIC Benchmarking to CVTR Test Data, Structure Temperature

6.10 Demonstration of the Method for Large and Small Breaks, Conservative Cases

The large and small steam pipe breaks presented in this section demonstrate the conservatism in the method. The [[

]] correlations are biased as described in Section 6.8.2.

6.10.1 Containment Response to Large Steam Pipe Break, Conservative Case

Containment pressure and temperature responses calculated by using the conservative case assumptions are compared to the results of the base case assumptions for a large steam pipe break shown on Figure 6-26 and Figure 6-27. The biases in the inputs and assumptions cause adding approximately [[ ]] to the peak pressure as shown on Figure 6-26. This difference decreases to approximately [[ ]] in four hours.

The peak containment pressure and temperatures are listed in Table 6-6.

The differences between the temperatures using base case and conservative case assumptions are not as large as the differences in the pressure. [[

]]

It can be concluded from the above observations that the biases used in the conservative cases add a significant margin to the peak pressure values. However, there is not a significant difference in the peak shell temperatures. The cooldown of the shell is slower in the conservative case as compared to the base case.

Containment gauge pressure decreases [[ ]] and shows a decreasing trend in the conservative case. In the base case, containment gauge pressure decreases [[ ]], and also shows a decreasing trend. [[

]] The heat load in the containment becomes small. In the absence of break flow, containment pressure continues to decrease [[ ]].

On Figure 6-28 through Figure 6-30, the conservative case results are compared to those obtained by using the Uchida correlation for condensation keeping all other inputs and assumptions the same. The difference in the peak pressure is negligible. [[

]] Because the PCCS surface temperature remains below the saturation temperature in the long term, condensation heat transfer to the PCCS continues. Because of the conservatism in the biased DLM correlation as compared to the Uchida correlation after the peak, the containment pressure decreases faster in the long term

in the BWRX-300 GOTHIC conservative case than it would if the Uchida correlation were also used.

Containment temperatures predicted by using the biased DLM correlation and Uchida correlation are compared on Figure 6-30. There is not a significant difference in the air temperatures. However, the shell temperatures show some differences in the very short-term. It should be noted that the shell inner and outer surfaces shown on Figure 6-30 are the maximum shell temperatures; they are not the average shell temperatures. Because the Uchida correlation does not include any information about the velocities near the wall, it cannot predict the high condensation heat transfer that occurs locally. As a result, Uchida correlation underpredicts the shell temperature while high velocities exist and misses the initial peak that occur in the shell temperature. However, shell temperatures predicted by the Uchida and the modified DLM correlations approach each other after the velocities subside.

The comparisons above show that the condensation model used in the BWRX-300 containment method represents the trends accurately, it applies a sufficient level of conservatism comparable to that predicted by the Uchida condensation heat transfer correlation that has been found to be acceptable by the NRC staff previously.

[[

]]

Figure 6-26: Containment Pressure Following a Large Steam Pipe Break, Comparison of Conservative and Base Cases [MaxP]

[[

]]

Figure 6-27: Containment Temperatures Following a Large Steam Pipe Break, Comparison of Conservative and Base Cases [MaxT]

[[

]]

Figure 6-28: Comparison of Containment Pressures Predicted by the Biased DLM and Uchida Correlations [MaxP]

[[

]]

Figure 6-29: Comparison of Heat Transfer Rates Predicted by Biased DLM and Uchida Correlations [MaxP]

[[

]]

Figure 6-30: Comparison of Containment Temperatures Predicted by the Biased DLM and Uchida Correlations [MaxT]

6.10.2 Containment Response to Small Pipe Breaks, Conservative Cases

The containment response predicted by using the conservative case assumptions for small pipe breaks is shown on Figures 6-31 through 6-34 for small steam pipe breaks and on Figures 6-39 through 6-41 for small liquid pipe breaks. [[

]]. The peak containment pressure and temperatures are listed in Table 6-6.

The maximum pressure on Figure 6-31 for the small steam break is well below the peak pressure resulting from a large steam break shown previously on Figure 6-26 and discussed in Section 6.10.1. The mass and energy release rate calculated by assuming no back pressure in Section 5.4 is used in the GOTHIC model to calculate the containment pressure. In reality, the break flow will start decreasing after it becomes unchoked as the containment pressure approaches the RPV pressure and will become very small when the RPV and containment pressures are nearly the same. After this time, mass discharge to the containment becomes small enough to maintain containment pressure slightly below the RPV pressure. If the mass discharge rate were to increase momentarily, containment pressure would increase above the RPV pressure and the mass discharge would stop again until the containment pressure returns to a value below the RPV pressure. Therefore, after the time that the RPV and containment pressures equalize, the upper bound for the containment pressure is the RPV pressure corresponding to the no-break case. The lower bound of the containment pressure is the containment pressure calculated by assuming no break flow after the time the RPV and containment pressures equalize. It should be noted that the lower bound for the containment pressure is discussed here to illustrate the trends but does not have any associated acceptance criteria. In reality, there may be other favorable conditions that may make the containment pressure lower than the values calculated here.

[[

]]

The PCCS exit temperature and the reactor cavity pool temperature are shown on Figure 6-32. PCCS #1 is the PCCS unit closest to the break location, PCCS #6 is the farthest. The steam volume fraction in the containment (excluding the dome region) is shown on Figure 6-33. The maximum steam volume fraction, which occurs in the higher sections of the containment, [[ ]], decreases slowly in the long term. Note that the calculations conservatively assume no heat loss from the reactor cavity pool to the surroundings through the walls. However, heat loss due to surface evaporation from the pool is taken into account.

The peak shell temperature shown on Figure 6-34 resulting from a small steam pipe break is comparable to the peak shell temperature resulting from a large steam pipe break shown on Figure 6-30, although the timing of the peak is much different.

As discussed in Section 5.4, containment pressure is assumed to be at atmospheric pressure to maximize the break flow rate. However, if the ICS can depressurize the RPV faster than the PCCS can depressurize the containment, it is conceivable that non-condensable gases in the containment will be ingested into the RPV and into the ICS heat exchangers. For all cases, the effect of nitrogen ingestion, if it does occur, is modeled for all components of the TRACG model (e.g., RPV, ICS, piping). As discussed in Section 5.2.4, TRACG is well qualified to predict the effects of non-condensable gases that may be ingested into the ICS. Build-up of non-condensable gases in the ICS heat exchangers may degrade the heat removal rate of the ICS, causing the system to re-pressurize again. This potential was investigated by performing an iteration between the TRACG calculations for a small steam pipe break accounting for the containment back pressure, and GOTHIC calculations for the containment using the modified break flow from TRACG. Note that the containment back pressure has no effect on the break flow rate until the break flow becomes unchoked. Therefore, the results of the cases with and without back pressure are identical while the break flow is choked. [[

]]

The RPV pressure, the containment pressure specified as back pressure in the break flow calculations, and the containment pressure calculated by GOTHIC are plotted on Figure 6-36. The difference between the RPV and containment pressures becomes progressively smaller with time, but the containment pressure always remains below the RPV pressure [[

]] As shown on Figure 6-37, there are no reversals in the break flow. As shown in the results without back pressure, the PCCS is capable of reducing the containment pressure well below the RPV pressure in the absence of break flow. Therefore, if the back pressure were to increase slightly above the RPV pressure, the break flow would stop, and containment pressure would decrease again. The total amount of nitrogen ingested into the RPV would be insignificant. The ICS heat exchangers are capable of removing decay heat in the presence of much higher levels of non-condensable gases as discussed in Section 5.2.4.

The effect of using the containment back pressure in calculating the break flow on the containment pressure is shown on Figure 6-38. [[

]]

The calculated peak containment pressure is not affected by the assumption made for containment pressure used to calculate the break flow because the break flow remains choked well past the time of the peak containment pressure for either assumption. Any impact on containment pressure occurs only in the long-term and is in the conservative direction when the containment back

pressure is not considered in the break flow calculation. The sensitivity case presented here shows that ignoring the back pressure increases the conservatism in the analysis.

Containment responses were calculated for small liquid pipe breaks until the RPV and containment pressures equalize. [[
]] The results are shown on Figures 6-39 through 6-42. The containment response trends for the liquid pipe breaks are similar to the small steam pipe breaks. After the RPV level falls below the break location, the break flow is fed from the steam space in the RPV and displays the characteristics of a small steam pipe break. Therefore, the trends observed in Figures 6-39 through 6-42 are consistent with the trends in steam pipe break shown in Figures 6-31 through 6-34.

[[

]]

Figure 6-31: Containment Pressure Following a Small Steam Pipe Break [MaxP]

[[

]]

Figure 6-32: PCCS Exit and Reactor Cavity Pool Temperatures Following a Small Steam Pipe Break, Conservative Case [MaxT]

[[

]]

Figure 6-33: Steam Volume Fraction in the Containment Following a Small Steam Pipe Break, Conservative Case [MaxP]

[[

]]

Figure 6-34: Containment Temperatures Following a Small Steam Pipe Break [MaxT]

[[

]]

Figure 6-35: Power, Small Steam Break, 2 ICS Trains, Conservative Case, with Containment Back Pressure Obtained from the MaxP Case

[[

]]

Figure 6-36: Pressure, Small Steam Break, 2 ICS Trains, Conservative Case, with Containment Back Pressure [MaxP]

[[

]]

Figure 6-37: Break Flow, Small Steam Break, 2 ICS Trains, Conservative Case, with Containment Back Pressure

[[

]]

Figure 6-38: Containment Pressure Using Break Flow With and Without Back Pressure [MaxP]

[[

]]

Figure 6-39: Containment Pressure Following a Small Liquid Pipe Break [MaxP]

[[

]]

Figure 6-40: PCCS Exit and Reactor Cavity Pool Temperatures Following a Small Liquid Pipe Break, Conservative Case [MaxT]

[[

]]

Figure 6-41: Containment Temperatures Following a Small Liquid Pipe Break [MaxT]

[[

]]

Figure 6-42: Steam Volume Fraction in the Containment Following a Small Liquid Pipe Break, Conservative Case [MaxP]

Table 6-6: Summary of the Peak Containment Pressure and Temperatures Calculated by Using the Conservative Assumptions

[[		
		]]

6.10.3 Containment Mixing for Combustible Gases

Hydrogen and oxygen generation results from radiolysis in BWRX-300 design basis accidents are discussed in Section 5.2.4. The radiolytic gases mixed in steam and liquid are discharged from the break along with the break flow. The volumetric fractions are calculated in Section 5.2.4. Hydrogen and oxygen distributions in the containment are not a concern for large breaks [[

]]. Radiolytic gases may build up in the containment following unisolated small breaks over time even though the rate of release is very small.

Total mass fraction of hydrogen and oxygen produced by radiolysis, remaining in the RPV and released to the containment are shown on Figure 6-43. [[

]]
Radiolytic gases mixed in steam enter into the dome region and condense on the containment dome, liberating the radiolytic gases mixed within. Although the volume fraction of radiolytic gases in the steam is small, it may accumulate in the dome region over time.

The radiolytic gas volume fractions are specified in the break flow boundary condition as calculated in Section 5.2.4, and radiolytic gas volume fraction distribution in the containment and the dome region was calculated for small steam pipe break case presented in Section 6.10.2.

Hydrogen volume fraction in the containment is shown on Figure 6-44. Hydrogen volume fraction in the dome region is higher than the main containment volume as expected, but the difference is not large. [[

]] The hydrogen volume fractions shown on Figure 6-44 are far below the deflagration limits even if there is sufficient oxygen.

Hydrogen and oxygen are generated at stoichiometric ratio from radiolysis; the molecular (or volume) ratio of radiolytic oxygen to hydrogen is 0.5. Because the radiolytic gases are well mixed in steam or liquid water where they are generated, the molecular or volume ratio of radiolytic oxygen to hydrogen remains 0.5 as they migrate in the RPV, from RPV to containment and within the containment. Therefore, radiolytic oxygen volume fraction in the containment is exactly half of the hydrogen volume fraction shown on Figure 6-44. There is also some small amount of oxygen initially present in the containment. [[

]]

The results presented here show that gases generated by radiolysis do not create a concern for deflagration in the containment and that the containment subcompartments remain sufficiently mixed.

[[

]]

Figure 6-43: Radiolytic Gas Generation and Release from RPV, Small Steam Pipe Break, 2 ICS Trains, Conservative Case

[[

]]

Figure 6-44: Hydrogen Volume Fraction in the Containment Main Volume and in the Dome Region, Small Steam Pipe Break, 2 ICS Trains, Conservative Case

6.11 Summary of the Assumptions and Inputs Used in the BWRX-300 GOTHIC Method Conservative Cases

The conservative containment response cases use the following inputs:

- Initial containment pressure is at the Technical Specification limit.
- Initial bulk containment temperature and the structures are at a reasonably low value that would occur during normal operation.
- Initial humidity in the containment is 20%.
- Reactor cavity pool temperature is at the Technical Specification limit.
- Bounding values are used for form loss coefficients in containment and in the PCCS units.
- Free space volume in the containment is conservatively calculated.
- The containment nodalization uses node sizes as presented in the base cases in this report.
- The initial airspace temperature above the reactor cavity pool is assumed to be the same as the pool water temperature.
- The initial relative humidity of the airspace is assumed to be 100%.

The conservative containment response cases use the following modeling parameters:

- [[ ]]
- Condensation and convection heat transfer correlations are biased as described in Section 6.8.2.
- [[

]]
- No credit is taken for heat transfer from the outer surface of the metal containment shell to the concrete or surroundings, except for heat transfer from the submerged section of the containment dome to the reactor cavity pool above the dome.
- The reactor cavity pool is modeled as a lumped parameter volume. The air space is connected to a constant pressure boundary condition such that the airspace pressure is nearly constant at atmospheric pressure.
- There is no heat loss from the pool to the walls. Surface evaporation from the pool is accounted for.
- Heat transfer coefficients on the containment shell, PCCS and containment dome are biased as described in Section 6.8.2.

7.0 REFERENCES

7.1 NEDC-33910P, BWRX-300 Reactor Pressure Vessel Isolation and Overpressure Protection

7.2 NEDC-33911P, BWRX-300 Containment Performance

7.3 Regulatory Guide 1.203, Revision 0, "Transient and Accident Analysis Methods," December 2005

7.4 Regulatory Guide 1.157, Revision 0, "Best-Estimate Calculations of Emergency Core Cooling System Performance," May 1989

7.5 NEDE-32176P, Revision 4, "TRACG Model Description," January 2008

7.6 NEDE-32177P, Revision 3, "TRACG Qualification," August 2007

7.7 NEDC-32725P, Revision 1, Volumes 1 and 2, "TRACG Qualification for SBWR," September 1997

7.8 NEDC-33080P, Revision 1, "TRACG Qualification for ESBWR," May 2005

7.9 NEDC-33005P-A, Revision 2, "TRACG Application for Emergency Core Cooling Systems / Loss-of-Coolant-Accident Analyses for BWR/2-6," May 2018

7.10 NEDC-33083P-A, Revision 1, "TRACG Application for ESBWR," September 2010

7.11 26A6642AT, Revision 10, "ESBWR Design Control Document, Tier 2, Chapter 6 Engineered Safety Features," GE Hitachi Nuclear Energy, April 2014

7.12 NUREG/CR-5249, Revision 4, "Quantifying Reactor Safety Margins: Application of Code Scaling, Applicability, and Uncertainty Evaluation Methodology to a Large-Break, Loss-of-Coolant Accident," October 1989

7.13 NEA/CSNI/R3(2014), "Containment Code Validation Matrix," May 2014

7.14 SMSAB-02-02, "An Assessment of CONTAIN 2.0: A Focus on Containment Thermal Hydraulics (Including Hydrogen Distributions)," July 2002

7.15 NEDC-33004P-A, Revision 4, "Constant Pressure Power Uprate," July 2003

7.16 GOTHIC Thermal Analysis Package Technical Manual, Version 8.3(QA), November 2018

7.17 GOTHIC Thermal Analysis Package Qualification Report, Version 8.3(QA), November 2018

7.18 Peterson, P.F., V.E. Schrock and T. Kageyama, "Diffusion Layer Theory for Turbulent Vapor Condensation with Noncondensable Gases," Transaction of ASME, Vol. 115, pp. 998-1003, November 1993

7.19 Bucci, Matteo, "Experimental and Computational Analysis of Condensation Phenomena for the Thermal-Hydraulic Analysis of LWRs Containments," PhD Thesis, University of Pisa, Italy, 2009

7.20 Bucci, Matteo, Walter Ambrosini and Nicola Forgione, “Experimental and Computational Analysis of Steam Condensation in The Presence of Air and Helium,” Nuclear Technology, Volume 181, pp. 115-132, January 2013

7.21 Cotton, M.A. and Jackson, J.D. “Vertical tube air flows in the turbulent mixed convection regime calculated using a low-Reynolds-number k~ ϵ model,” International Journal of Heat and Mass Transfer, Volume 33, Issue 2, pp. 275-286, February 1990

7.22 Idaho Nuclear Corporation Report IN-1403, “Simulated Design Basis Accident Tests of the Carolinas Virginia Tube Reactor Containment Final Report,” December 1970. NRC Adams Accession Number: ML12009A104